

Annual and monthly analysis of surface urban heat island intensity with respect to the local climate zones in Budapest



Csenge Dian^{a,*}, Rita Pongrácz^{a,b}, Zsuzsanna Dezső^a, Judit Bartholy^{a,b}

^a Department of Meteorology, Eötvös Loránd University, Budapest, Hungary

^b Faculty of Science, Excellence Center, Eötvös Loránd University, Mártonvásár, Hungary

ARTICLE INFO

Keywords:

Urban Heat Island
Satellite data
MODIS
Surface temperature
Local climate zones
Central Europe

ABSTRACT

Built-up areas with non-natural surface covers generate the urban heat island (UHI) effect. To investigate this in greater spatial extensions, satellite data provide sufficient spatial coverage without unnecessary time lag effect within the region. Moreover, it is very costly to operate a meteorological station system with a suitable density. Although the cost of maintaining satellites is also high, however, a lot of satellite data is available free of charge to users. For instance, surface temperature data derived from MODIS (Moderate Resolution Imaging Spectroradiometer) measurements can be used to obtain surface temperature-based UHI (SUHI) intensity. Due to the variability of built-up density and vegetation cover within the city, different subregions can be characterized by the Local Climate Zone (LCZ) system. The main goal of the paper is to analyse the relationship between the SUHI intensity and the LCZ classes for Budapest. SUHI intensity values were determined relative to the average surface temperature of the surrounding rural areas. Our conclusions clearly show that as building density decreases, the SUHI intensities also decrease. The highest intensities can be found in the city centre, and the lowest SUHI intensities with negative values (i.e. adverse or cooling effect) appear in vegetation-covered LCZ classes. The SUHI intensity variability is generally greater in summer than winter, which can be detected in case of all LCZ classes due to the substantial difference of incoming solar radiation.

1. Introduction

The proportion of the urban population is increasing nowadays, about the half of the world total population already lives in cities (UN, 2015). This urban/rural ratio is higher in more developed countries, and it is approximately 70% in Hungary (HCSO, 2017, <https://www.ksh.hu/>). Artificial surface covers, buildings and human activities concentrating in cities significantly modify the radiation components of energy budget and near surface wind thus creating the unique climate of cities. The urban climate is determined by the built-up density, which mainly depends on the population and the urban structure. The most often mentioned element of the urban climate is the urban heat island (UHI) effect, which refers to the temperature difference between the densely built-up inner areas of the city and the vicinity outside the city (Oke, 1973). This temperature difference can be defined as the UHI intensity. In order to determine this intensity, it is certainly important to define and separate urban and rural sections within the target area (Stewart, 2007).

The UHI can already be detected in cities with 5000 inhabitants in Europe (Landsberg, 1981), nevertheless, the UHI intensity is clearly greater in larger cities. More specifically population density has a close relationship to building density and the overall city

* Corresponding author.

E-mail address: diancsenge@caesar.elte.hu (C. Dian).

structure. Structural characteristics, i.e. the ratio of artificial and natural surfaces, substantially influence the UHI intensity. Another example is the canyon geometry, which modifies the radiation conditions by multiple reflections, absorptions and reemissions (Oke, 1981). The vegetation generally cools its vicinity due to the evapotranspiration, which requires energy from the environment. This cooling effect is determined by the height, spatial extension, type (e.g. deciduous or evergreen) and overall structure of the vegetation (Yu and Hien, 2006; Cohen et al., 2012).

Two fundamental research methods can be distinguished in studying the UHI: (i) in situ air temperature measurements and (ii) surface temperature data derived from satellite measurements (Voogt and Oke, 2003). Although air temperature is used more commonly (e.g. Klysik and Fortuniak, 1999; Unger, 2004; Kolokotroni and Girdharan, 2008; Gál et al., 2016; Pongrácz et al., 2016), the appropriate coverage of a larger area can be a problem, which is not the case when using remotely-sensed satellite data (e.g. Tran et al., 2006; Pongrácz et al., 2010; Dousset et al., 2011). The daily distributions of UHI intensities are different when using the different methods, thus it is very important to highlight whether air or surface temperature is used. The air temperature-based UHI intensity reaches its maximum at night (Oke, 1982), while the maximum of the surface temperature-based UHI (SUHI) occurs in the very early afternoon when the incoming solar radiation is the greatest (Vukovich, 1983). The UHI intensity varies within the city, the maximum value usually occurs in the central densely built-in part, whereas SUHI intensity reflects more the materials of different surface cover types due to their radiation characteristics. Both building density and surface cover are considered in Local Climate Zones (LCZs) defined by Stewart and Oke (2012). The LCZ system focuses on the microclimatic conditions within the city, dividing it into different groups (including natural and artificial covers) on the basis of meteorological considerations. LCZ classifications are increasingly used in Europe and Asia for UHI intensity studies based on either air temperature (e.g. Leconte et al., 2015) or surface temperature (e.g. Kaloustian and Bechtel, 2016). LCZ maps for two Hungarian cities, namely, Budapest and Szeged are available (Unger et al., 2014). In this study, the SUHI intensities of Budapest are analysed and compared for the different LCZ classes. Moreover, LCZs can be incorporated into different models to characterize the urban areas. For instance, Alexander et al. (2015) used an energy balance model to analyse Dublin and its vicinity, which can be characterized by wet climatic conditions with a strong oceanic influence; or Brousse et al. (2016) used the Weather Research and Forecasting (WRF) model especially for the urban environment in the case of Madrid, a typical Mediterranean agglomeration.

Here the focus is on a Central/Eastern European city with an overall continental climate. In this region, many urban climate studies were already carried out. Air temperature researches were conducted in Poland (Beranová and Huth, 2005) and Romania (Croitoru et al., 2012); and satellite analysis in several cities in Romania (Cheval and Dumitrescu, 2015; Herbel et al., 2017) and the Czech Republic (Dobrovolný, 2013). Berenová and Huth (2005) showed that the increase of the UHI intensity based on air temperature depends on the circulation and the direction of the airflow. According to satellite data, the SUHI intensity shows asymmetry in Cluj Napoca (Romania), although the surface coverage is similar on the eastern and western sides of the city. Furthermore, during the extremely severe heat wave period the SUHI intensity was weak (Herbel et al., 2017). Dobrovolný (2013) showed that the SUHI intensity of Brno (Czech Republic) can be up to 4–7 °C. LCZ maps of many Central European cities have been prepared, for example Szeged (Hungary), Brno (Czech Republic), Bratislava (Slovakia), Kraków (Poland) and Vienna (Austria) (Bokwa et al., 2018); Novi Sad (Serbia) (Savić et al., 2013); Cluj-Napoca (Romania) (Herbel et al., 2016) and Olomouc (Czech Republic) (Lehnert et al., 2015). The urban climate of these cities was studied on the basis of LCZ maps and air temperature data or modelling. Both the studies of Herbel et al. (2016) and Lehnert et al. (2015) found the highest UHI intensities in the most densely built-up LCZ class, which can be expected as the artificial cover with specific radiation characteristics is more dominant in these areas.

The novelty of this research is that the LCZ map is combined with satellite surface temperature data in Budapest (the capital of Hungary, which has not been studied from this aspect, yet) using specific criteria to match their spatial resolutions and the limitations stemming from cloud cover. Specifically, the objectives of this paper are: (1) to determine the distribution of the LCZ categories in Budapest using gridded satellite data, (2) to investigate the SUHI intensity of Budapest in the various LCZ categories using annual, seasonal and monthly scales, (3) to compare different sectors classified as a particular LCZ class, and (4) to evaluate a case study for the evolution of the spatial structure of SUHI intensity.

2. Data and methodology

For analysing the relationship between the SUHI intensity from satellite data and the LCZ map of Budapest it is certainly necessary to examine them together.

2.1. Satellite data

We aim to study the entire area of the city at the same time in this urban climate research. This requires a very dense meteorological measurement network, but at least one station must represent each type being present in the city (Alexander et al., 2015; Gál et al., 2016). Such measurement network is not available in the current investigation area, Budapest. Therefore, in this case it is preferable to use satellite data, which instantly covers a large area. This choice of using satellite measurements implies that we investigate the SUHI intensity based on the derived surface temperature, thus we must focus on more or less clear-sky conditions.

The thermal infrared channels of the different sensors are used to determine the satellite surface temperature. These sensors are available on satellites with either geostationary (e.g. METEOSAT, GOES) or polar orbit (NOAA, MetOp, Landsat, Terra, Aqua). Sensors on geostationary satellites can be better applied on global scale because of possible direct world-wide comparability. Landsat-8 data can be used for spatial analysis, but its application is limited due to calibration problems. The resolution of the ASTER sensor (on satellite Terra) is sufficiently fine (90 m), but it only operates for a limited part of the entire orbit and provides occasional

measurements for a specific region, thus ASTER is not suitable for time series analyses. The resolution of the MODIS (Moderate Resolution Imaging Spectroradiometer) sensor (1 km) is already suitable for urban scale analysis of large agglomerations. Moreover, time series of almost two decades are available, ideally with four data daily (Rasul et al., 2017), and the UHI of many European cities has been studied with MODIS surface temperature data (Schwarz et al., 2011). Operational polar satellites used traditionally in synoptic meteorology and weather forecasts (e.g. NOAA or MetOp satellite series) do not provide finer resolution data compared to MODIS and use fewer infrared channels for the measurements.

Satellites Terra and Aqua were launched as the part of the American National Aeronautics and Space Administration's (NASA) Earth Observing System (EOS) in December 1999 and May 2002, respectively. They both are on ~705 km height polar orbits around the Earth with an inclination of 98°. Their orbital periods are approximately 100 min, so they orbit the Earth 16 times a day. Both satellites are sun-synchronous, Terra crosses the Equator on a descending orbit at 10:30 a.m., whereas Aqua crosses it on an ascending orbit at 1:30 p.m. They pass over most of the Earth surfaces twice in a day. Except the polar region, which is covered at each orbit. Satellite Terra passes over the Budapest agglomeration area in around 9–10 UTC (NASA, 1999) and 20–21 UTC, while satellite Aqua flies above this target area at around 02–03 UTC and 12–13 UTC (NASA, 2002). Five instruments were installed in satellite Terra and six in satellite Aqua.

The sensor MODIS is one of them that can be found on both satellites. It measures 36 electromagnetic spectral bands, from visible (405–40 nm) to infrared (14085–14,385 nm). To calculate the SUHI intensity the Land Surface Temperature (LST), and Land Cover (LC) MODIS products (Strahler et al., 1999) are used. The LC is necessary in this study to determine the vegetation-covered and built-up areas. In addition, seven infrared channels (i.e. channels 20, 22, 23, 29, 31, 32, 33 using 3660–3840 nm, 3929–3989 nm, 4020–4080 nm, 8400–8700 nm, 10,780–11,280 nm, 11,770–12,270 nm, 13,185–13,485 nm bands, respectively) are used to determine the LST with 1 km resolution, derived by the method of Wan and Snyder (1999). The LST fields can be downloaded from the LP DAAC (Land Processes Distributed Active Archive Center) from 2001 till present. LST represents the active surface which is the cloud top in the case of cloudy conditions, thus representing missing information from the point of view of the continental surface. This way the SUHI intensity can be calculated for cloudless pixels using the average rural LST. In this paper, we use the monthly average and individual SUHI intensity fields.

2.2. Locale climate zone map of Budapest

The main goal of the local climate classification is to characterize the microclimate of different urban structures. For this purpose, Stewart and Oke (2012) identified several parameters for classifying the local climatic zones. Seven parameters represent the geometry and surface cover properties (i.e. the sky view factor, aspect ratio, building surface fraction, impervious surface fraction, pervious surface fraction, height of roughness elements, terrain roughness class) and three parameters are used for thermal, radiative, and metabolic properties (i.e. surface admittance, surface albedo, anthropogenic heat output). The detailed analyses of these parameters and characteristical values are discussed in the urban climate literature (e.g. Auer, 1978; Grimmond and Oke, 1999). All together seventeen LCZs were determined based on the values of the parameters. Ten classes among them depend on the height and density of the buildings, and some land use properties (e.g. heavy industry areas), these classes are the built types, numbered from LCZ 1 to LCZ 10 (Table 1, column 1). Oke (2004) previously already created urban climate zones, which correspond to the LCZ 1–LCZ 9. Another seven classes were created according to the surface cover types, named as LCZ A through LCZ G (Table 1, column 2). These surface cover types depend on the height and type of vegetation (e.g. trees, shrubs, low plants), vegetation density and soil coverage (paved surface, sand, rock). The actual LCZ class can be compiled from more than one class when a more complex area is defined. In addition, four more variable land cover properties can be used to refine the LCZ classes, e.g. bare trees (in case of deciduous trees in winter) or snow cover (Table 1, column 3). All the megacities can be categorized with this LCZ classification system, which enables us to identify common features (Planning Department, 2012).

Bechtel et al. (2015) created a commonly used method, which allows to prepare the LCZ map of any city. The detailed description of this method and the resulting maps are summarised on the WUDAPT's (World Urban Database and Access Portal Tool) website (<http://www.wudapt.org/>). WUDAPT (2019) is an international initiative, which aims to collect data on the structure and functioning of cities around the world. Many cities are already mapped with the required data sets are available on this website, thus further analyses on the basis of the LCZ maps can be carried out (e.g. Cai et al., 2016). The LCZ maps of other cities can be created

Table 1

The seventeen local climate zones (LCZ) classes (Stewart and Oke, 2012) based on geometry, surface cover properties and thermal, radiative, metabolic properties.

Built types	Land cover types	Additional subtypes with variable land cover properties
LCZ 1: compact high-rise	LCZ A: dense trees	b: bare trees
LCZ 2: compact midrise	LCZ B: scattered trees	s: snow cover
LCZ 3: compact low-rise	LCZ C: bush, scrub	d: dry ground
LCZ 4: open high-rise	LCZ D: low plants	w: wet ground
LCZ 5: open midrise	LCZ E: bare rock or paved	
LCZ 6: open low-rise	LCZ F: bare soil or sand	
LCZ 7: lightweight low-rise	LCZ G: water	
LCZ 8: large low-rise		
LCZ 9: sparsely built		
LCZ 10: heavy industry		

using the detailed instructions included on the website. Several cities, including Budapest, were already classified with this WUDAPT-recommended method for the 9th International Conference on Urban Climate (ICUC9) held in Toulouse in summer 2015.

The maps of two Hungarian cities, namely the capital (Budapest) and the third most populated city (Szeged) are already created (Gál et al., 2015). We use the LCZ map of Budapest in this study. Because of the regional characteristic not all the 17 LCZ classes can be found in Budapest, for instance the highest building is 88 m tall (only the domes of the Parliament building and a cathedral reach this height), which can be found in a University campus in the southeastern central part of the city. However, this is a unique building and it is not occupied the characteristic unit size that is generally used in LCZ classification. The common height of the tall buildings in Budapest is about 30 m, therefore similarly to other Central European cities (e.g. Bokwa et al., 2018) LCZ 1 does not appear in the LCZ map of the Hungarian capital. The seven LCZ classes being present in Budapest are as follows:

- LCZ 2: Compact midrise
- LCZ 5: Open midrise
- LCZ 6: Open low-rise
- LCZ 8: Large low-rise
- LCZ A: Dense trees
- LCZ D: Low plants
- LCZ G: Water

2.3. Methodology

The relationship between the LCZ map and the SUHI intensity is analysed here for Budapest. The SUHI intensity are derived from the data of sensor MODIS between January 2001 and October 2016. The urban and rural grid cells are separated in the target area in order to calculate SUHI intensity as the difference between the LST of the actual grid cell and the average of the rural grid cells (rural grid cells are defined according to Pongrácz et al. (2010), namely, where non-built-up land cover is present around the city within the city-size vicinity, and the elevation difference above sea level from the city's average elevation do not exceed ± 100 m). Fig. 1a shows the location of the urban (red) and rural (green) grid cells.

The LCZ map of Budapest, (2017) (http://geopedia.world/#T4_L107_x2130299.9783078623_y6020180.347740481_s11_b17) is transformed for a $70 \times 70 \text{ km}^2$ domain of the MODIS grid cells, which include Budapest and its agglomeration. Both the LCZ map and the MODIS grid domain are shown on the Google Earth (2017) map (<https://earth.google.com>) in Fig. 1b. For the current study the MODIS grid cells within the administrative boundaries of Budapest are used. Note that the spatial resolution of the LCZ map (250 m) is finer than the MODIS grid (1 km), therefore an LCZ class should be assigned to the coarser MODIS grid cells that include several LCZ categories. To define this properly, three slightly different criteria are introduced.

We define three criteria for LCZ coverage and three criteria for cloud cover, which are well suited to the urban structure and local climate of Budapest.

So the analysis includes the following two main steps:

- to determine the LCZ class for each MODIS grid cell,
- to determine cloud coverage criteria.

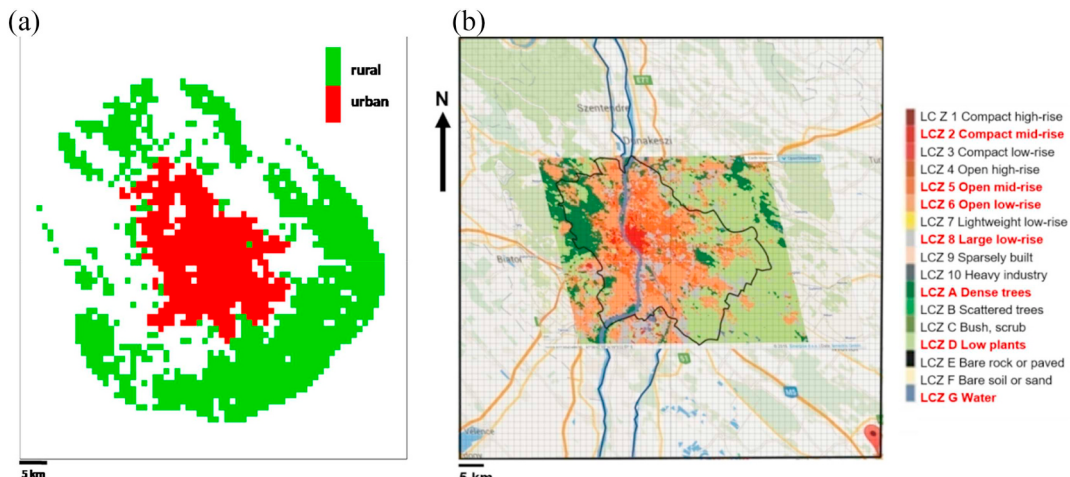


Fig. 1. (a) The urban (red) and rural (green) grid cells of the $70 \times 70 \text{ km}^2$ domain based on Pongrácz et al. (2010). The rural grid cells were used as the actual reference to define the SUHI intensity. (b) The local climate zone map of Budapest transformed to the MODIS grid ($70 \times 70 \text{ km}^2$ domain). LCZ types appearing in Budapest and its close vicinity are highlighted with red. (For interpretation of the references to colour in this figure legend, the reader is referred to the web version of this article.)

The first step determines the characteristical LCZ class of each MODIS grid cell covering 1 km² using the following three criteria defined in this study:

LCZ Class criterion 1 (LC1): the dominant LCZ is considered in the grid cell, independently from the extent of the actual coverage of the different LCZ classes present within the grid cell;

LCZ Class criterion 2 (LC2): the LCZ, which covers at least 50% of the grid cell;

LCZ Class criterion 3 (LC3): the LCZ, which covers at least 75% of the grid cell.

These LC1, LC2, LC3 series of criteria correspond to the urban structure of Budapest, but can be generalized and applied to other cities. For this purpose, the percentages of LCZ coverage vary depending on the heterogeneity of the urban area. For example, in a city with extended homogeneous units, districts, stricter conditions (e.g. at least 75% or even 100% coverage of an individual LCZ class) can be applied to an appropriate analysis, because there will be sufficient number of grid cells for such analysis.

The second step determines the cloud cover of the total 70 × 70 km² target domain. Cloud cover is an important factor in satellite measurements because the sensor does not measure the continental surface in cloudy weather. If a substantial part of the study area is covered by cloud then the average temperatures of urban and rural grid cells limited to the cloud-free parts only and thus they do not represent the entire target area. Three cloud cover criteria are defined and applied in this study depending on the extent of cloud cover:

Cloud Cover criterion A (CCA): < 25% of the grid cell is covered with cloud.

Cloud Cover criterion B (CCB): < 10% of the grid cell is covered with cloud.

Cloud Cover criterion C (CCC): 0% of the grid cell is covered with cloud (cloudless days).

The applicability of the cloud cover criteria depends greatly on local climatic conditions. In regions where cloud coverage is generally lower (e.g. the Mediterranean region), stricter criteria may be used because of less cloudy days. However, there are other areas where the cloud cover extends over much larger portion of the whole agglomeration than in the case of Budapest (e.g. along the Atlantic coastline), or it is considered quite typical throughout the year, thus more days with partial cloud cover should be included in the analysis to have an appropriate number of grid cells for completing the research.

It is important to note that in the days corresponding to the CCA and CCB criteria, the cloud-covered grid cells were omitted from the calculations (both averages and frequencies).

Table 2 summarises the frequency of total days relative to the whole period of the study (and also per season) using the three cloud cover criteria. Since the daytime measurements represent the highest SUHI intensities (Pongrácz et al., 2010), the Terra's morning and Aqua's afternoon measurements are compared here. In general, more cases can be included in the analysis when using the measurements of satellite Terra than Aqua, which is partly due to the afternoon convection resulting in cumulus clouds. It is important to mention that cloudless days are very rare only about 4–5% of the total days, the most of them occur in summer and these days cannot be found in winter.

To define SUHI intensity the Terra satellite's morning and evening measurements were used between January 2001 and October 2016, and the Aqua satellite's afternoon and dawn data between January 2003 and October 2016. We calculated annual and monthly averages, seasonal distributions, full time series and monthly frequencies when using the different CC criteria.

3. Results and discussion

All the three cloud cover criteria were used in the LCZ class-wise analysis of SUHI intensity for Budapest. Here results using CCA are discussed in the cases of annual and seasonal scale analyses, which are followed by the monthly scale evaluation using CCB. Finally, the temporal evolution of the spatial structure of SUHI intensity is shown in a cloudless period (i.e. using CCC).

Table 2

Frequency of days relative to the entire length of measurement period (Terra's morning measurements in the period of 2001–2016, Aqua's afternoon measurements in the period of 2003–2016) with each cloud cover criterion (i.e. CCA, CCB, CCC). Besides the whole year (third column), seasonal proportions (the four columns in the right) are also given.

Cloud cover	Proportion of total days				
	Total days	Winter days	Spring days	Summer days	Autumn days
CCA: < 25%	Terra a.m.	33%	16%	35%	47%
	Aqua p.m.	28%	12%	30%	39%
CCB: < 10%	Terra a.m.	26%	10%	28%	38%
	Aqua p.m.	20%	9%	23%	26%
CCC: = 0%	Terra a.m.	5%	0%	5%	8%
	Aqua p.m.	4%	0%	3%	6%

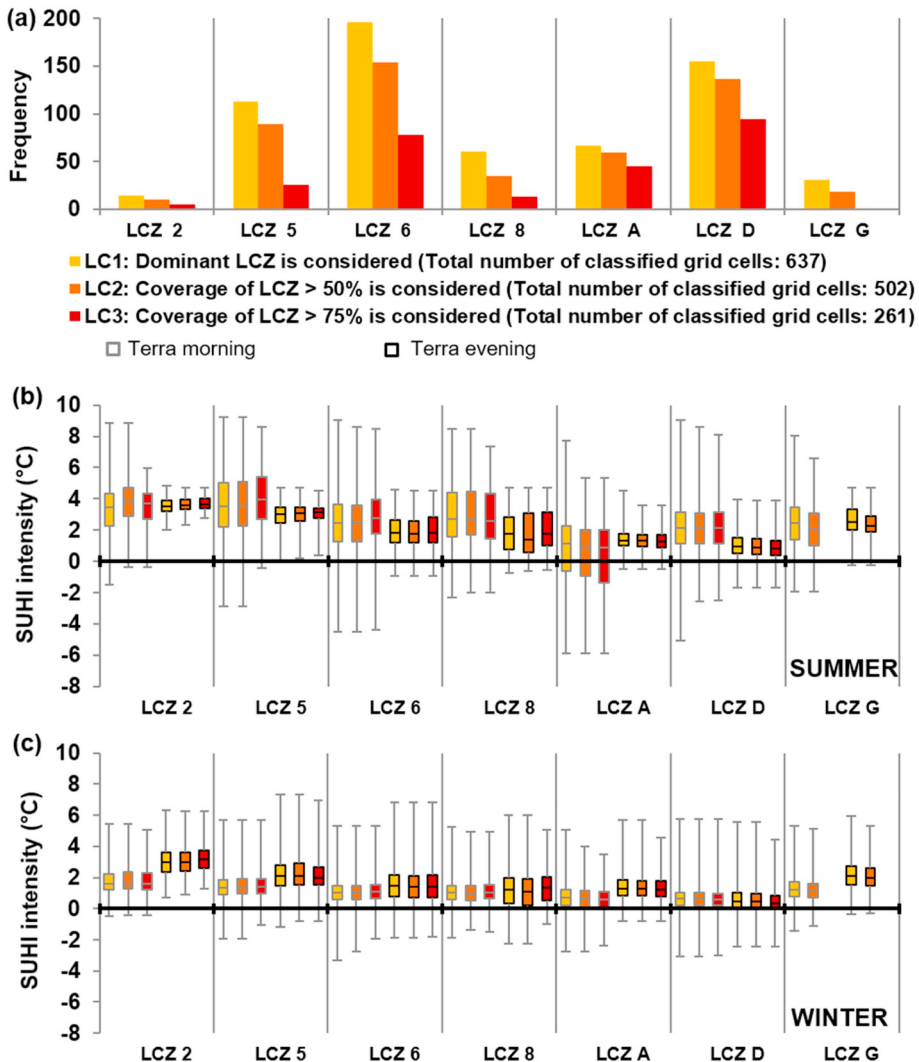


Fig. 2. The distribution of MODIS grid cells according to the LCZ types in Budapest based on the three criteria (a). The distribution of the heat island intensity (Box-Whisker diagrams indicate the minimum, lower quartile, median, upper quartile, maximum of monthly averages) in the different LCZ categories based on the Terra's morning (grey boxes) and evening (black boxes) measurements in summer (b) and winter (c), 2001–2016.

3.1. The distribution of the monthly average SUHI intensities

Fig. 2a summarises the number of grid cells belonging to the given LCZ class according to the three defined criteria, i.e. LC1, LC2, LC3. All the grid cells can be classified according to LC1, and as the criterion becomes stricter, both the total number of classified grid cells and the results for the numbers of grid cells in individual LCZ classes decrease. So LCZ G cannot be identified at all using LC3 due to the difference between MODIS grid sizes and the characteristical spatial extensions of the Danube (width of the riverbed) and the open water surfaces of city lakes. The largest lake of Budapest is the Lake Naplás (a flood control reservoir of Szilas creek located in the eastern part of the city), which covers around 1 km² total area shared by two different MODIS grid cells.

Most of the grid cells belong to LCZ 6 (open low-rise) according to LC1 and LC2, while the maximum number of grid cells occurs in LCZ D (low plants) when using the LC3. The minimum number of grid cells can be found in LCZ 2 (compact midrise), only about 2% of total classified grid cells according to the actual criterion because this type is dominant quite homogeneously in the ~10 km² extension of the city centre (small patches can be found in the western side with < 1 km² altogether) and therefore the aggregation to the MODIS grid does not affect substantially the final classification.

To illustrate the distribution of the SUHI intensity within the individual LCZ classes we used Box-Whiskers diagrams. The box indicates the middle 50% of the data between the lower and upper quartiles, the middle line shows the median, and the vertical thin lines are drawn between the maximum and minimum values. Fig. 2b summarises the SUHI intensity distribution of Terra's morning (grey boxes) and evening (black boxes) measurements for the three different criteria in summer. The main conclusions from this diagram are as follows: (i) The total intervals of the SUHI intensities are much wider in the morning than in the evening. (ii) Only

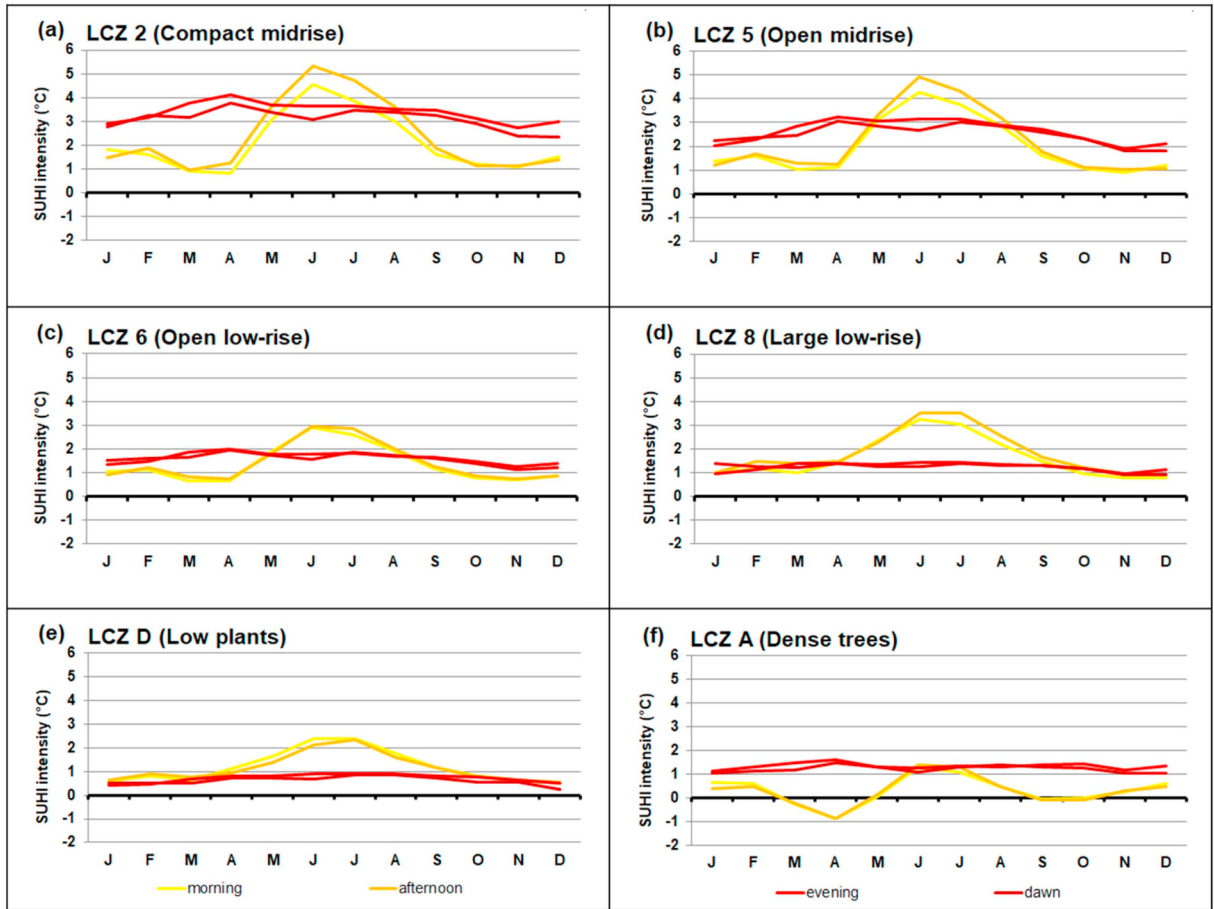


Fig. 3. Annual distribution of monthly median of heat island intensity (2001–2016) over individual LCZ classes during the four satellite measurement time (evening and morning from Terra, dawn and afternoon from Aqua).

positive intensities can be found in the LCZ 2 and LCZ 5, which include the most densely built-in areas of Budapest. (iii) $> 25\%$ of the data are negative in LCZ A (dense trees) using either criterion. (iv) Substantial differences can be recognised between the three criteria mostly when looking at the minimum and maximum values in LCZ 2, LCZ 5, LCZ A, and LCZ D. Fig. 2c shows the SUHI intensity distribution in winter similarly to the middle panel. The morning intensities include narrower intervals, while the evening values form wider intervals in winter than summer. Unlike in summer the actual time within the day does not affect the entire intensity distribution in winter since the morning and evening SUHI intensity values fall into very similar ranges.

For further analyses presented in this paper we use the LC2, thus very inhomogeneous grid cells were excluded, but a sufficient number of grid cells still remained for the study.

3.2. Average annual distribution of the median of SUHI intensity

The aim of this section is to investigate the annual distribution of SUHI intensity. Since there is a chance that the actual SUHI intensity series are not normally distributed, so the monthly median values are evaluated here. In order to analyse the annual distribution of SUHI intensity, monthly median values were calculated over each LCZ class using LC2 and CCA. Since we have four different satellite passes the difference between surface temperature values can be evaluated. Shortwave solar radiation determines LST in daytime that it is not available in night-time so long wave radiation is the only source of the radiation budget. The consequent difference between daytime and night-time average SUHI intensities can be seen in Fig. 3. However, morning and afternoon (or evening and dawn) measurements do not result substantially different annual distribution. Nevertheless, daytime SUHI intensities show clearly recognised annual distribution than night-time SUHI intensities, when monthly median values are within only 1 °C range throughout the whole year for each LCZ class. The highest night intensity occurs in LCZ 2 (compact midrise) and the lowest in LCZ D (low plants). The highest daytime SUHI intensity occurs in summer, also in LCZ 2, the densely built-up areas of Budapest.

The summer daytime maximum of intensity implies that SUHI is determined by the incoming solar radiation, which is the greatest when it reaches the surface with the highest angle. In contrast, the maximum UHI intensities based on air temperature occur in clear nights because of the higher heat storage of non-natural cover compared to vegetation or bare soil. However, the spatial patterns of

nighttime UHI and daytime SUHI intensities are similar, namely, the highest intensity values occur in the most densely built-in parts of the city with the highest buildings (i.e. LCZ1 and LCZ2) as it was concluded in the studies of [Lehnert et al. \(2015\)](#) and [Herbel et al. \(2016\)](#) in case of air temperature based analysis. Our results are also consistent with these results although surface temperature is used.

In general, peak SUHI intensity values decrease with the decreasing built-up density. The lowest average intensities, which are in fact negative values, occur in LCZ A (dense trees), indicating that the forested areas of Budapest are cooler in spring and autumn than the rural surroundings.

3.3. Comparison of grid cells classified to the same LCZ class

Different LCZ class are compared in sections 3.1. and 3.2., here the time series of the SUHI intensity are compared in selected MODIS grid cells from the same LCZ class. The purpose of this chapter is to understand how the SUHI intensity is affected by the location of the grid cell within the city. This viewpoint facilitates the understanding of various factors (beyond the LCZ category) influencing SUHI intensity. [Fig. 3](#) clearly shows that the maximum SUHI intensity occurs in summer afternoon, that is why the afternoon measurements (12–13 UTC) of Aqua are used for the comparison in this section, so the time series covers the period 2003–2016.

The selection of the grid cells is based on the following three criteria:

- the given LCZ class covers the entire grid cell;
- the entire grid cells from the same LCZ class should be as far from each other as possible;
- the vicinity of the selected grid cells should belong to the same LCZ class as the selected ones as much as possible.

In this paper, we present the time series of monthly SUHI intensity in eight selected grid cells, for the 2003–2016 period. [Table 3](#) summarises the selected grid cells and [Fig. 4](#) provides their geographical locations in the LCZ map of Budapest.

The relationship between the two time series is characterized by the root-mean-square error (RMSE) and the linear correlation coefficient (r). To calculate the RMSE the well-known Eq. (1) is used, where x_{1i} and x_{2i} are the individual values of the corresponding grid cells' time series, and n is the length of the entire time series (that equals here to 166 as the number of months from January 2003 to October 2016). Due to this definition, smaller RMSE indicates a greater similarity between the time series.

$$RMSE = \sqrt{\frac{\sum_{i=1}^n (x_{1i} - x_{2i})^2}{n}} \quad (1)$$

The LCZ 2 mainly occurs more or less homogeneously in the city centre of Budapest. Due to the extension of this $\sim 10 \text{ km}^2$ central area the two selected grid cells are located close to each other. That is why their time series are similar (RMSE = 0.052 °C, $r = 0.94$). Noticeable differences (1.5–2 °C) between these two time series can be detected in the summers of 2011 and 2016 ([Fig. 5a](#)). The maximum SUHI intensities generally exceed 5 °C, and even 7 °C in 2005, 2006, and 2008.

Two grid cells were selected from LCZ 5 (open midrise), Újpest (3) from northern Budapest and Csepel (4) from southern Budapest. The SUHI intensity values are generally higher in Csepel during the entire period (RMSE = 0.165 °C), which is probably due to the different surroundings of the two grid cells. More specifically, Újpest (3) is located in a residential area surrounded (i) mainly by the same LCZ 5 and (ii) secondarily by the somewhat lower buildings of LCZ 6, in contrast, Csepel (4) is located in a more heterogeneous part of the city where extended brownfield lands (LCZ 8) can also be found nearby, and they cause higher SUHI intensity in Csepel (4) compared to Újpest (3). Despite the 1.7 °C average shift ([Fig. 5b](#)) between the two time series the highly similar annual distribution causes high correlation value ($r = 0.81$).

Most of the grid cells belong to the LCZ 6 (open low-rise) within Budapest as it can be seen in [Fig. 2a](#). Among them Kispest (5) from eastern plain part, and Budatétény (6) from the western hilly part of the city are selected. The SUHI intensity is generally stronger in Kispest than in Budatétény (RMSE = 0.135 °C), however, similar annual distributions of SUHI intensity results a high correlation of the time series ($r = 0.79$) ([Fig. 5c](#)). Intensity values are somewhat smaller in LCZ 6 than in either LCZ 2 or LCZ 5, the summer maximum values usually do not exceed 6 °C. In the case of Budatétény negative intensities occurred during several spring

Table 3

The LCZ type, name and location (latitude, longitude) of the selected grid cells for the local comparison analysis. The location of the selected cells is shown in [Fig. 4](#).

Grid cell	LCZ type	Name (location)
1	LCZ 2: Compact mid-rise	City Centre, North (47.512°N, 19.153°E)
2		City Centre, South (47.495°N, 19.165°E)
3	LCZ 5: Open mid-rise	Újpest (47.562°N, 19.165°E)
4		Csepel (47.437°N, 19.190°E)
5	LCZ 6: Open low-rise	Kispest (47.454°N, 19.240°E)
6		Budatétény (47.429°N, 19.128°E)
7	LCZ A: Dense trees	Csillebér (47.504°N, 19.054°E)
8		Budapesti Kamaraerdő (47.445°N, 19.103°E)

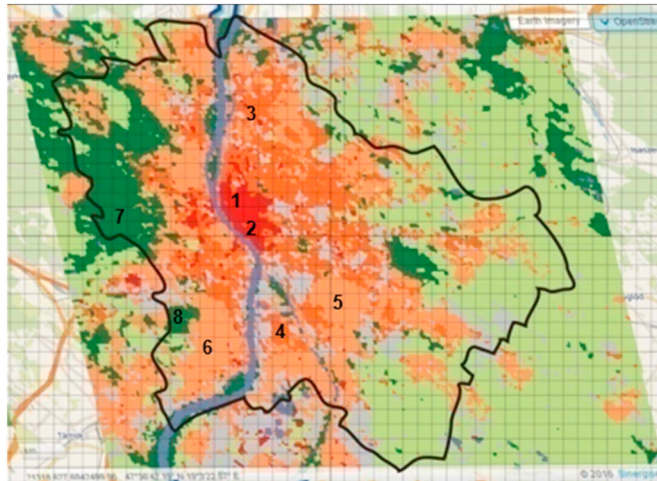


Fig. 4. The location of the grid cells within Budapest, which were selected for the comparison (1 and 2 - LCZ 2: Compact mid-rise; 3 and 4 - LCZ 5: Open mid-rise; 5 and 6 - LCZ 6: Open low-rise; 7 and 8 - LCZ A: Dense trees). More details are provided in [Table 3](#).

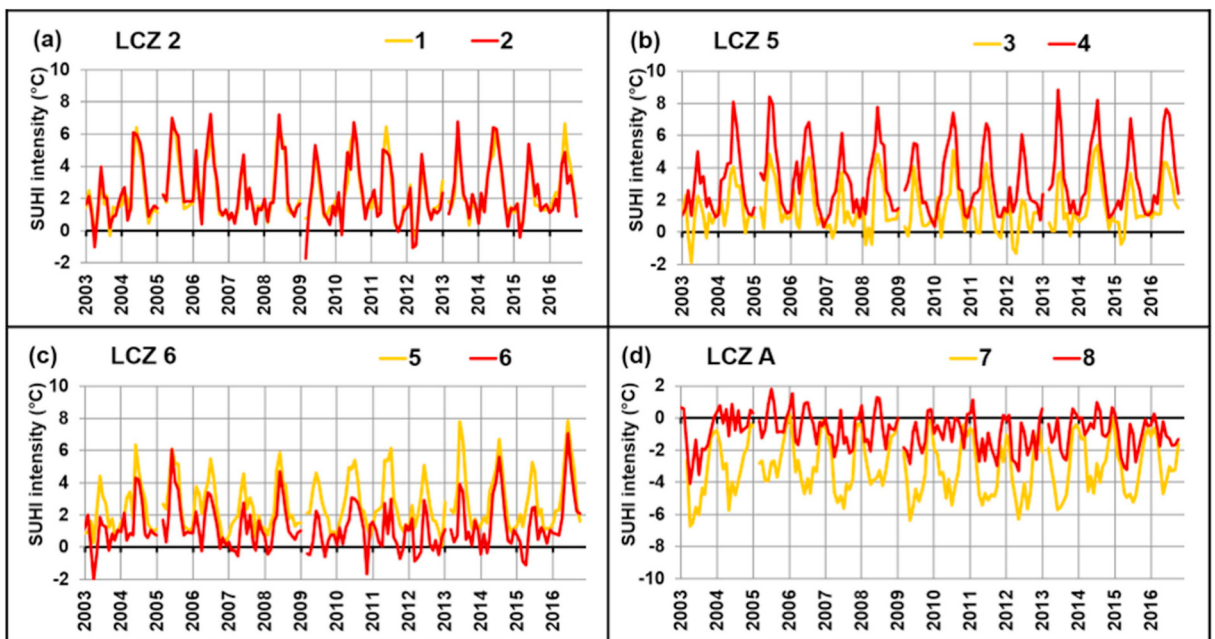


Fig. 5. Comparison of the monthly heat island intensity time series in the eight selected grids cells ([Table 3](#) and [Fig. 4](#) show the location of the grid cells in Budapest) based on the Aqua afternoon measurements from January 2003 to October 2016.

and autumn months, which is probably due to the relative closeness of forest area.

Among the vegetation covered classes, LCZ A (dense trees) is selected, represented by two grid cells from the north-western and south-western parts of the city: Csillebér (7) is located in a larger forested area at 400–450 m above sea level, and the Budapesti Kamaraerdő (8) forms a smaller forest area at 100–200 m above sea level. As [Fig. 5d](#) shows, the calculated monthly average SUHI intensities are always negative in the entire period 2003–2016 in Csillebér (7), indicating a clear cooling effect to the city. SUHI intensities are also mostly negative in the Budapesti Kamaraerdő (8), however, their cooling effect is less than in Csillebér (7). The RMSE of these two time series (0.208 °C) is the greatest and the correlation is the smallest ($r = 0.53$) among the grid cell pairs representing different LCZ classes. The difference between the two time series of LCZ A is due to the different heights above sea level and the different extent of the forested areas.

These results clearly show the difference between the different classes, namely, SUHI intensity reaches higher values (especially in summer) in more densely built-up areas, whereas vegetation cover has an opposite effect to SUHI intensity (and result in mainly lower LST values compared to the rural average) due to the substantially different radiation characteristics of vegetation compared to non-natural surfaces with buildings. Moreover, the difference within an individual LCZ class can also be seen well. This difference

reflects the overall extension of the given LCZ class (beyond a single grid cell) and the other LCZ classes by which the selected grid cell is surrounded or that are embedded within the greater extent of the given LCZ class.

3.4. Histograms of monthly SUHI intensity

After the detailed analysis of monthly SUHI intensity values calculated as the averages of individual SUHI intensity fields, a statistical frequency analysis is added using the individual measurements. Here we used the criterion CCB. Since the maximum SUHI intensity occurs in daytime, this analysis focuses on daytime measurements. Moreover, the Terra passes over the target region at around 9–10 UTC, while the Aqua measurements represent the early afternoon (at 12–13 UTC) conditions. Since the convection is stronger in the afternoon, which imply that more clouds form, and the number of potential days are less than in the morning that is why we use the Terra's morning measurements to show the relative frequency of the monthly SUHI intensities of two very different LCZ classes (Fig. 6). One of them is LCZ 2 (compact mid-rise), the most densely built-in class among all the classes that appear in Budapest, and the other is LCZ A (dense trees), the most vegetation-covered class. The middle 50% between the upper and lower quartiles of the total frequency distribution is highlighted in the monthly diagrams by the horizontal lines near the x axis with the corresponding colours. It is important to note the substantial difference between the total numbers of analysed days in the different months. For instance, only 40–60 days are available in the winter months according to the cloud cover criterion due to the more often occurrence of cloudy weather and fog. Less cloud cover results in much more cases (i.e. 140–230 days/month) in summer.

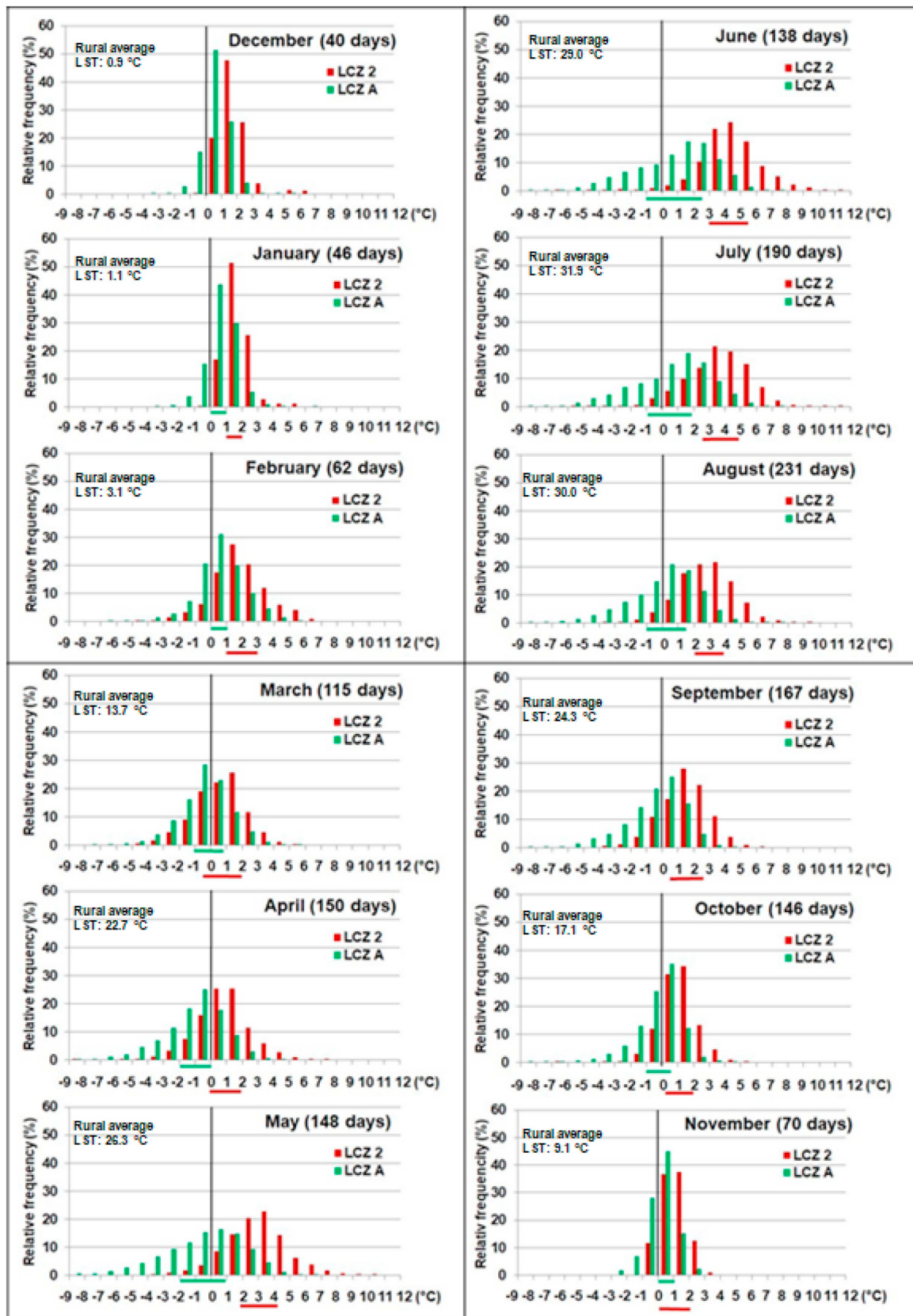
The relative frequencies of the monthly SUHI intensity substantially differ in the winter half-year from the summer half-year. The SUHI intensities cover narrow intervals from October to January, therefore the highest relative frequencies (> 50%) occur in December and January. The most often occurring SUHI intensities can be found around 0–1 °C in LCZ A and 1–2 °C in LCZ 2 in these winter months. The SUHI intensity intervals are wider from February to September, and the maximum variability occurs in summer. Consequently, the relative frequencies of the intervals decrease, the highest frequencies are only 20–25% in these months. Negative SUHI intensity (implying lower LST compared to the rural average) occurs more frequently in LCZ A in spring, which highlight the cooling effect of vegetation. The SUHI intensity mostly exceeds 3 °C (sometimes reaches 10 °C) in the city centre (LCZ 2) in June and July (the exceedance frequency is > 80% and 65%, respectively). Thus, the annual development of SUHI intensity is well separated in these two LCZ classes. Clearly higher SUHI intensities are detected in built-up areas than in vegetation-covered areas. Surface temperature is basically determined by solar radiation in addition to the albedo and other radiation characteristics of the surface. The highest incoming radiation occurs in summer due to the highest solar elevation angle. Thus, the difference of surface temperature values of different land cover areas are the most pronounced in summer. Furthermore, in winter the deciduous vegetation is less able to exert its mitigating effect. The variation of SUHI intensity within both class and month is also greater in summer than in winter, which is also due to the higher incoming solar radiation. Moreover, the summer half-year shows special characteristics in the distribution of SUHI intensities of LCZ A, namely, the histograms are somewhat skewed towards the negative values (forming the left tail of the distribution) from late spring until mid-Autumn. This can probably be explained by the extension and tree density of cells within LCZ A, as well as the mixture of different trees and other species being present in the area. This asymmetry is the most obvious in summer, when the canopy is fully developed and has the most effective cooling effect.

3.5. Case study for a cloudless period

Finally, the temporal evolution of the SUHI intensity spatial structure was investigated during a fairly long period of cloudless days over the entire $70 \times 70 \text{ km}^2$ domain. Only 4–5% of the total days fulfils this criterion from the 14–16 years analysed period, mostly in summer (August). Cloudless days did not occur in winter at all, which is due to the geographical characteristics (i.e. located in a large basin) of the target area. Low level stratus cloud, fog and inversion often occur in Hungary during anticyclone period in winter. In contrast, there are typically very few clouds in the anticyclonic periods in summer. Thus, solar radiation in summer is higher than in winter and the difference between various surface types also appears better. Moreover, extreme warm conditions (such as heat waves resulting in heat stress and further health consequences on the human body) tend to occur during such anticyclonic conditions in summer. The frequency of extreme weather situations are generally projected to increase due to global climate change (IPCC, 2012). Since more heat wave periods can be expected in the region of the Budapest agglomeration in the 21st century (e.g., Pongracz et al., 2013; Pieczka et al., 2018), therefore it is important to analyse specific examples of such conditions in urban areas in order to better understand how the temperature conditions develop in the city during heat waves. This helps scientists and decision makers to develop appropriate adaptation strategies on local level.

This is why the selected period is a four-day-long heat wave event occurred in 26–29 August 2016, when eight cloudless measurements are available from the morning (Terra) and afternoon (Aqua) passes. A multicentre cyclone system dominated western and northern Europe during this period, while an anticyclone can be observed over southern and central Europe (Fig. 7). The temperature was 30–35 °C due to the advection of dry and warm air in Hungary (Fig. 8).

Fig. 9 summarises the evolution of the SUHI intensity spatial structure at the four selected days in the entire $70 \times 70 \text{ km}^2$ domain. The Danube can be well recognised in the maps because it is cooler than the vicinity areas due to the slower daily warming of water. In the morning of 26.08.2016 (Fig. 9a) the SUHI intensity is weak; the maximum value is 5 °C and it occurs in a very small area (in the southern part of the central districts). Then, in the afternoon and the following morning, SUHI intensified and the maximum values exceeded 7 °C, which appeared in the geographical center of the city (Fig. 9b and 9.c), northwest from the maximum SUHI intensity values in the morning of 26 August. After this two time steps the SUHI intensity of the city center reduced from the early afternoon of 27 August (Fig. 9d) to the afternoon of 29 August (Fig. 9h), a secondary short intensification of SUHI occurred in the afternoon of 28



(caption on next page)

Fig. 6. Relative frequency of the monthly SUHI intensities of the LCZ 2 (Compact mid-rise), and LCZ A (Dense trees) classes using the Terra's morning measurements, 2001–2016. The total number of days with available data (using CCB cloud cover criterion, < 10% of the grid cells covered with cloud over the whole Budapest agglomeration area) are shown in parentheses after the name of the month. The middle 50% of the distribution is highlighted by the horizontal lines near the x axis (red for LCZ 2, green for LCZ A). The average of rural reference (monthly average LST) is given in the upper left corner of each diagram. (For interpretation of the references to colour in this figure legend, the reader is referred to the web version of this article.)

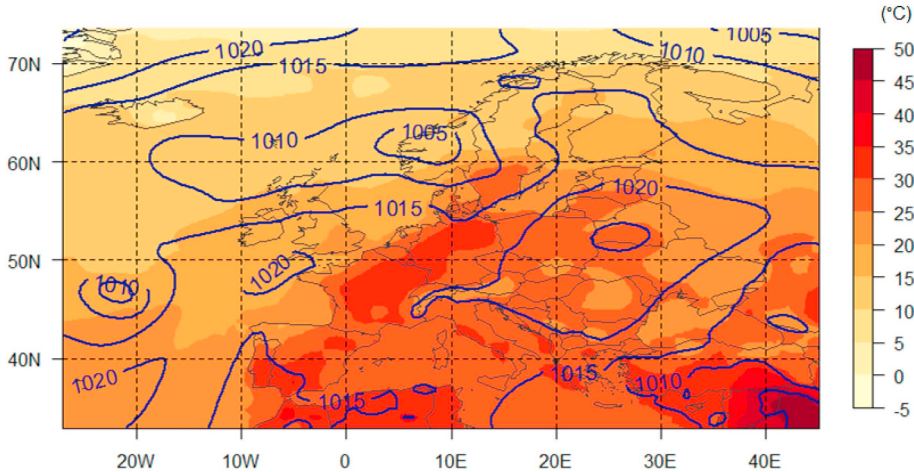


Fig. 7. Air temperature (°C, indicated by colours) and mean sea level pressure (hPa, indicated by isolines) in Europe, 12 UTC 26.08.2016. based on ERA Interim Database, [ECMWF \(2016\)](#).

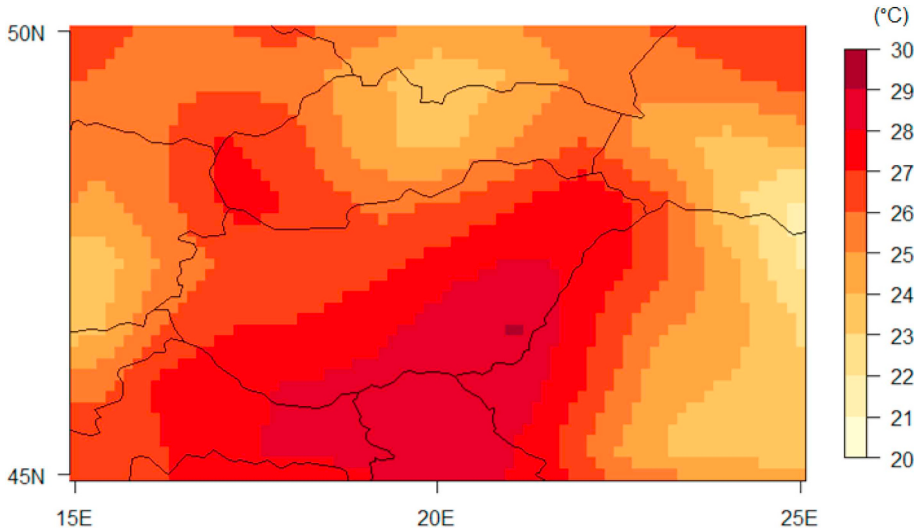
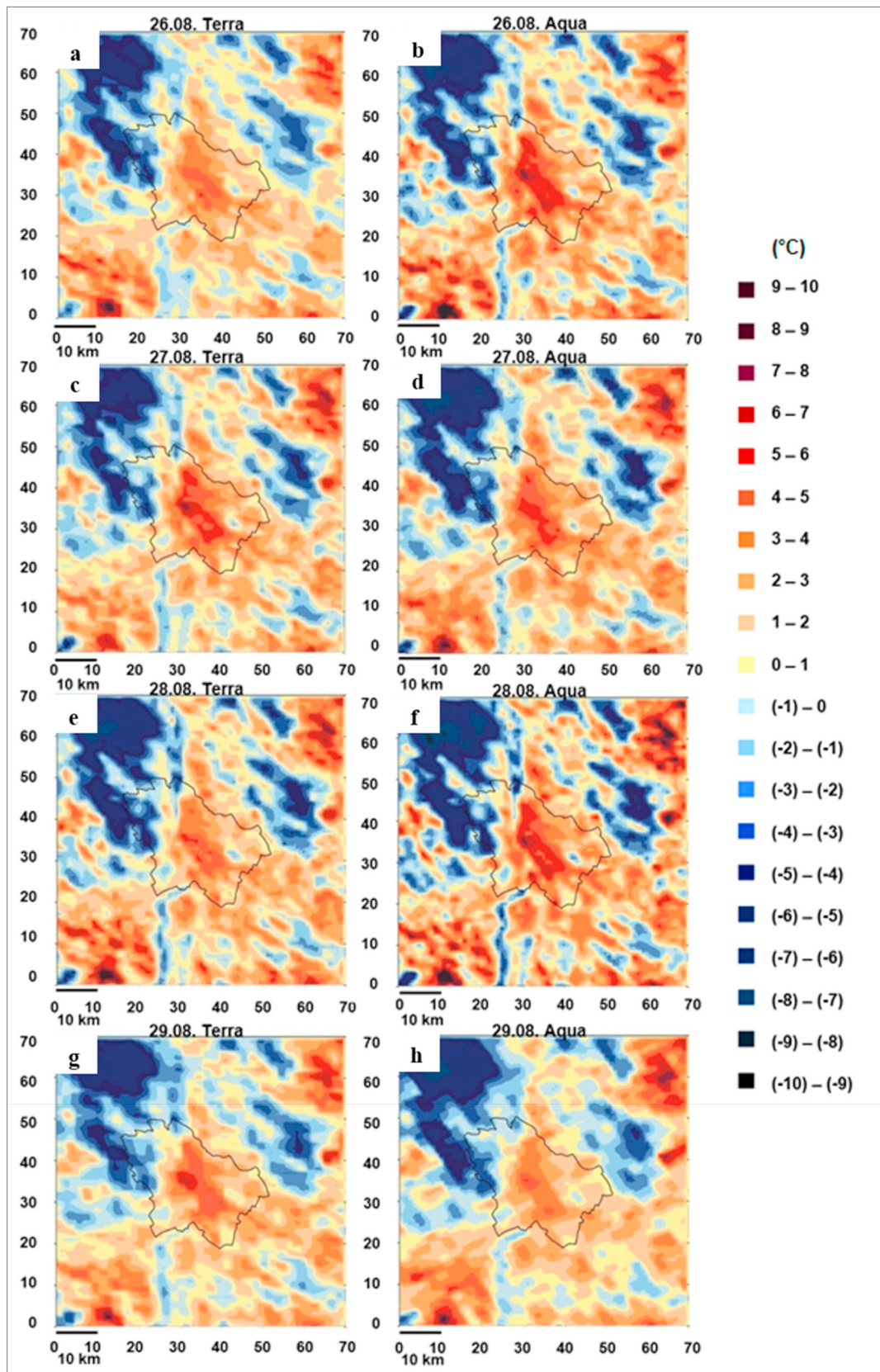


Fig. 8. Air temperature (°C) in Hungary, 12 UTC 26.08.2016. based on ERA Interim Database, [ECMWF \(2016\)](#).

August, with similar maximum intensity values in the city center than two days earlier (Fig. 9b). At the end of the four-day period, the anticyclone began to decay. The maximum SUHI intensity in the morning of 29 August in the city center is still strong (reaching 6 °C as Fig. 9g shows), but it substantially decreases by the afternoon. Overall, the highest SUHI intensities occur in the city centre (7–8 °C) during these four days, whereas the lowest intensities (negative intensity values) can be found in the Buda Hills in the western part of the city. In addition to the Buda Hills, the public cemetery (which is the largest cemetery in Budapest with an area of ~2 km² covered with trees) at the Pest side (eastern part) also shows negative SUHI intensity values throughout the entire period. The negative intensity values of the forested area of both the Buda Hills and the cemetery clearly show that the increase of green areas could mitigate the SUHI effect of Budapest and reduce the overall heat stress in the city.

It is well known that temperature pattern is influenced by advection. During the presented case study, the dominant wind direction was northern in Budapest based on the data of SYNOP reports ([Synop Reports, 2016](#)). This can be considered typical because of the flow direction of the river Danube that divides the city. The different surface covers (represented by the LCZ classes), the urban



(caption on next page)

Fig. 9. Evolution of the SUHI intensity spatial structure for the entire $70 \times 70 \text{ km}^2$ domain of Budapest and the agglomeration area, based on Terra's morning (left: a, c, e, g) and Aqua's afternoon (right: b, d, f, h) measurements in the period 26–29 August 2016.

structure (i.e. the spatial distribution pattern of LCZ classes) and the advection (wind direction) together resulted in the detected SUHI intensities. Specifically, three different LCZ classes are compared with a Box-Whiskers diagram in this period (Fig. 10). In order to avoid the overemphasis of the extreme SUHI intensities, the 5% and 95% percentiles are used to determine the whiskers of the diagram instead of minimum and maximum values. In addition, Fig. 10 also shows the upper and lower quartiles as well as the median for. LCZ 2, the compact midrise buildings, which can mostly be found in the centre of Budapest, LCZ 6 (open low-rise), most of the grid cells in Budapest are classified into this class, and LCZ A (dense trees) the forested areas of Budapest. The highest SUHI intensities ($> 6^\circ\text{C}$) occurred on 26th and 28th, in the afternoon. The SUHI intensities are always positive in LCZ 2, and around 50% of the values are negative in LCZ A at each individual satellite pass. The frequency distribution of LCZ 6 is dominantly ($> 75\%$) in the positive SUHI intensity range, thus the boxes of LCZ 6 in Fig. 10 are clearly between LCZ 2 and LCZ A. The comparison of these LCZ classes highlights the radiation differences between them, namely, the denser the buildings, the more intense the SUHI, and the more vegetation, the less intense the SUHI with a substantial cooling effect to the environment.

4. Conclusions

The dependence of the SUHI intensity on the LCZ classes was studied within Budapest, the capital city of Hungary with overall mid-latitude continental climatic conditions. The urban climate of Budapest has not been previously studied based on the LCZ system. In the surrounding countries, LCZ maps were compared with air temperature or model data. Therefore, a new approach is that we have used surface temperature data for the studies.

LST time series measured by sensor MODIS of satellite Terra (from January 2001 to October 2016) and Aqua (from January 2003 October 2016) served as basis to determine SUHI intensities as difference between the actual LST of the given grid cell and the rural mean LST. In addition, three types of CC criteria were defined (as described in section 2.3). Each MODIS grid cell in the Budapest agglomeration area was classified into a specific LCZ class using three LC criteria (also defined in section 2.3). The LC2 criterion was used in this paper for the analyses. We compared the average annual distributions of monthly mean SUHI intensity for different LCZ classes representing built-up areas at different degree and vegetation. More specifically, the summer and winter distributions of SUHI intensity are compared. The variability within the LCZ classes is illustrated by comparing the monthly SUHI intensity time series of selected grid cells within a given LCZ. Based on the analysis presented in this paper the following main conclusions can be drawn. (i) The highest SUHI intensities with around 5°C occur in LCZ 2 (compact midrise) located as a $\sim 10 \text{ km}^2$ block in the centre of Budapest, to the east from the Danube. (ii) As build-up density decreases the SUHI intensities also decrease. (iii) Negative average SUHI intensities occur in LCZ A, i.e. the vegetation-covered class. (iv) The monthly relative frequency distributions of the daily SUHI intensity values are compared here for these two classes, which differ the most from each other. Besides the shift of the frequency distribution towards greater SUHI intensity values in LCZ 2 relative to LCZ A, SUHI intensity values cover wider intervals in the summer months, whereas the total ranges are much narrower in winter months.

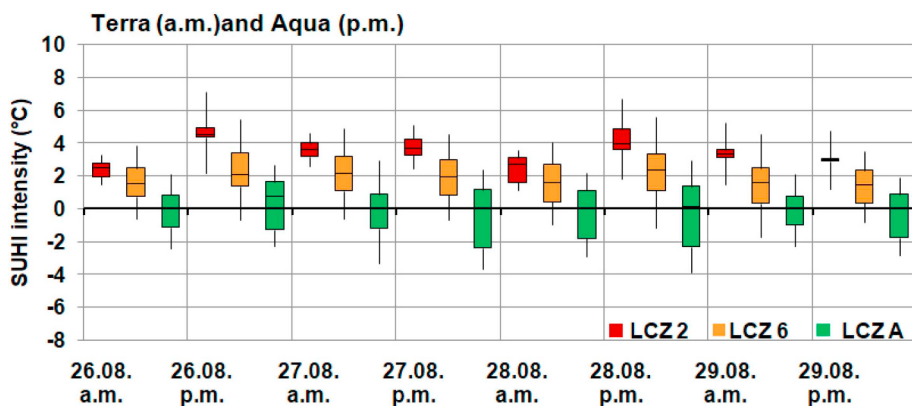


Fig. 10. The distribution of heat island intensity (using Box-Whisker diagram showing the 5% percentile, lower quartile, median, upper quartile, 95% percentile indicated by the lower end of the whiskers, the lower, middle, upper level of the box, and the upper end of the whiskers, respectively) in LCZ 2 (Compact mid-rise), LCZ 6 (Open low-rise) and LCZ A (Dense trees) classes based on Terra's morning and Aqua's afternoon measurements, 26–29 August 2016.

Acknowledgements

The authors wish to thank NASA for producing the satellite surface temperature data in their present form and the Earth Observing System Data Gateway for distributing the data. Research leading to this paper has been supported by the following sources: the Hungarian National Research, Development and Innovation Fund under grants K-120605, K-129162 and K-109109, the Ministry of National Development of the Hungarian Government via the AGRÁRKLIMA2 project (VKSZ_12-1-2013-0034), and the Széchenyi 2020 programme, the European Regional Development Fund and the Hungarian Government via the AgroMo project (GINOP-2.3.2-15-2016-0028).

References

- Alexander, P.J., Mills, G., Fealy, R., 2015. Using LCZ data to run an urban energy balance model. *Urban Clim.* 13, 14–37. <https://doi.org/10.1016/j.ulclim.2015.05.001>.
- Auer, A.H., 1978. Correlation of land use and cover with meteorological anomalies. *Journal of Appl. Meteorol.* 17, 636–643. [https://doi.org/10.1175-0450\(1978\)017<0636:COLUAC>2.0.CO;2](https://doi.org/10.1175-0450(1978)017<0636:COLUAC>2.0.CO;2).
- Bechtel, B., Alexander, P.J., Böhner, J., Ching, J., Conrad, O., Feddema, F., Mills, G., See, L., Stewart, I.D., 2015. Mapping local climate zones for a worldwide database of the form and function of cities. *ISPRS Int. J. Geo-Information* 4, 199–219. <https://doi.org/10.3390/ijgi410199>.
- Beranová, R., Huth, R., 2005. Long-term changes in the heat island of Prague under different synoptic conditions. *Theor. Appl. Climatol.* 82, 113–118. <https://doi.org/10.1007/s00704-004-0115-y>.
- Bokwa, A., Dobrovolný, P., Gál, T., Geletič, J., Gulyás, Á., Hajto, M.J., Holec, J., Hollósi, B., Kielarl, R., Lehnert, M., Skarbit, N., Šťastný, P., Švec, M., Unger, J., Walawender, J.P., Živela-Aloise, M., 2018. Urban climate in central European cities and global climate change. *Acta Climatol.* 51–52, 7–35. <https://doi.org/10.14232/acta.clim.2018.52.1>.
- Brousse, O., Martilli, A., Foley, M., Mills, G., Bechtel, B., 2016. WUDAPT, an efficient land use producing data tool for mesoscale models? Integration of urban LCZ in WRF over Madrid. *Urban Clim.* 17, 116–134. <https://doi.org/10.1016/j.ulclim.2016.04.001>.
- Cai, M., Ren, C., Xu, Y., Dai, W., Wang, X.M., 2016. Local climate zone study for sustainable megacities development by using improved WUDAPT methodology – a case study in Guangzhou. *Procedia Environ. Sci.* 36, 82–89. <https://doi.org/10.1016/j.proenv.2016.09.017>.
- Cheval, S., Dumitrescu, A., 2015. The summer surface urban heat island of Bucharest (Romania) retrieved from MODIS images. *Theor. Appl. Climatol.* 121, 631–640. <https://doi.org/10.1007/s00704-014-1250-8>.
- Cohen, P., Potchter, O., Matzarakis, A., 2012. Daily and seasonal climatic conditions of green urban open spaces in the Mediterranean climate and their impact on human comfort. *Build. Environ.* 51, 285–295. <https://doi.org/10.1016/j.buildenv.2011.11.020>.
- Croitoru, A.E., Holobaca, I.H., Lazar, C., Moldovan, F., Imbroane, A., 2012. Air temperature trend and the impact on winter wheat phenology in Romania. *Clim. Chang.* 111, 393–410. <https://doi.org/10.1007/s10584-011-0133-6>.
- Dobrovolný, P., 2013. The surface urban heat island in the city of Brno (Czech Republic) derived from land surface temperatures and selected reasons for its spatial variability. *Theor. Appl. Climatol.* 112, 89–98. <https://doi.org/10.1007/s00704-012-0717-8>.
- Dousset, B., Gourmelon, F., Laaidi, K., Zeghnoun, A., Giraudet, E., Bretin, P., Maurid, E., Vandendorren, S., 2011. Satellite monitoring of summer heat waves in the Paris metropolitan area. *Int. J. Climatol.* 31, 313–323. <https://doi.org/10.1002/joc.2222>.
- ERA Interim Database, ECMWF, 2016. <http://apps.ecmwf.int/datasets/data/interim-full-daily/>.
- Gál, T., Bechtel, B., Unger, J., 2015. Comparison of two different Local Climate Zone mapping methods. In: ICUC9 conference extended abstracts. Toulouse, France, 20–24.07.2015, Paper. http://www.meteo.fr/icuc9/LongAbstracts/gd2-6-1551002_a.pdf.
- Gál, T., Skarbit, N., Unger, J., 2016. Urban heat island patterns and their dynamics based on an urban climate measurement network. *Hungarian Geographical Bull.* 65 (2), 105–116. <https://doi.org/10.15201/hungeobull.65.2.2>.
- Google Earth, 2017. <https://earth.google.com/>.
- Grimmond, C.S.B., Oke, T.R., 1999. Aerodynamic properties of urban areas derived from analysis of surface form. *J. Appl. Meteorol.* 38, 1262–1292. [https://doi.org/10.1175/1520-0450\(1999\)038<1262:APOUAD>2.0.CO;2](https://doi.org/10.1175/1520-0450(1999)038<1262:APOUAD>2.0.CO;2).
- Herbel, I., Croitoru, A.E., Rus, I., Harpa, G.V., Ciupertea, A.F., 2016. Detection of atmospheric urban heat island through direct measurements in Cluj-Napoca city, Romania. *Hungarian Geographical Bull.* 65 (2), 117–128. <https://doi.org/10.15201/hungeobull.65.2.3>.
- Herbel, I., Croitoru, A.E., Rus, A.V., Roșca, C.F., Harpa, G.V., Ciupertea, A.F., Rus, I., 2017. The impact of heat waves on surface urban heat island and local economy in Cluj-Napoca city, Romania. *Theor. Appl. Climatol.* 133, 681–695. <https://doi.org/10.1007/s00704-017-2196-4>.
- Hungarian Central Statistical Office, Hungary 2017: <https://www.ksh.hu/> http://www.ksh.hu/docs/hun/xftp/terstat/2017/03/06_ts570304.pdf
- IPCC, 2012. Managing the risks of extreme events and disasters to advance ClimateChange adaptation. A special Report of working groups I and II of the Intergovernmental panel on climate change [Field, C.B., V. Barros, T.F. Stocker, D. Qin, D.J. Dokken, K.L. Ebi, M.D. Mastrandrea, K.J. Mach, G.-K. Plattner, S.K. Allen, M. Tignor, and P.M. Midgley (eds.)]. Cambridge University Press, Cambridge, UK, and New York, NY, USA, pp. 582.
- Kaloustian, N., Bechtel, B., 2016. Local Climatic Zoning and Urban Heat Island in Beirut. In: 4th International Conference on Countermeasures to Urban Heat Island (UHI) 2016. *Procedia Engineering.* 169, pp. 216–223. <https://doi.org/10.1016/j.proeng.2016.10.026>.
- Klysik, K., Fortuniak, K., 1999. Temporal and spatial characteristics of the urban heat island of Lódz, Poland. *Atmosph. Environ.* 33, 3885–3895. [https://doi.org/10.1016/S1352-2310\(99\)00131-4](https://doi.org/10.1016/S1352-2310(99)00131-4).
- Kolokotroni, M., Giridharan, R., 2008. Urban heat island intensity in London: an investigation of the impact of physical characteristics on changes in outdoor air temperature during summer. *Sol. Energy* 82 (2008), 986–998. <https://doi.org/10.1016/j.solener.2008.05.004>.
- Landsberg, H.E., 1981. The Urban Climate. Academic Press, pp. 275. <https://doi.org/10.1002/qj.49710845719>.
- LCZ map of Budapest, 2017. Geopedia. http://geopedia.world/#T4_L107_x2130299.9783078623_y6020180.347740481_s11_b17.
- Leconte, F., Bouyer, J., Claverie, R., Pétrissans, M., 2015. Using local climate zone scheme for UHI assessment: evaluation of the method using mobile measurements. *Build. Environ.* 83, 39–49. <https://doi.org/10.1016/j.buildenv.2014.05.005>.
- Lehnert, M., Geletič, J., Husák, J., Vysoudil, M., 2015. Urban field classification by “local climate zones” in a medium-sized Central European city: the case of Olomouc (Czech Republic). *Theor. Appl. Climatol.* 122, 531–541. <https://doi.org/10.1007/s00704-014-1309-6>. https://www.nasa.gov/pdf/156294main_terra_sw_guide.pdf.
- NASA, 1999. Science writers' guide to Terra. NASA EOS Project Science Office, Greenbelt, MD, pp. 28.
- NASA, 2002. Science writers' guide to Aqua. NASA EOS Project Science Office, Greenbelt, MD, pp. 32. https://aqua.nasa.gov/sites/default/files/references/Aqua_Sci_Writer%27s_Guide.pdf.
- Oke, T.R., 1973. City size and the urban heat island. *Atmos. Environ.* 7, 769–779. <http://www.theurbanclimatologist.com/uploads/4/4/2/5/44250401/post6oke1973uhiscaling.pdf>.
- Oke, T.R., 1981. Canyon geometry and the nocturnal urban heat island: comparison of scale model and field observations. *J. Climatol.* 1, 237–254. <https://doi.org/10.1002/joc.3370010304>.
- Oke, T.R., 1982. The energetic basis of the urban heat island. *Q. J. R. Meteorol. Soc.* 108, 1–24. <https://doi.org/10.1002/qj.49710845502>.
- Oke, T.R., 2004. Initial guidance to obtain representative meteorological observations at urban sites. Instruments and observing methods Report81, WMO/TD-No. 1250, 47. www.wmo.int/pages/prog/www/IMOP/publications/IOM-81/IOM-81-UrbanMetObs.pdf.
- Pieczka, I., Pongrácz, R., Bartholy, J., Szabóné, André K., 2018. Future temperature projections for Hungary based on RegCM4.3 simulations using new representative concentration pathways scenarios. *Int. J. Global Warming* 15, 277–292. <https://doi.org/10.1504/IJGW.2018.093121>.

- Planning Department, 2012. Urban Climatic Map and Standards for Wind Environment – Feasibility Study. FINAL REPORT; School of Architecture, CUHK, Hong-Kong, 518. http://www.pland.gov.hk/pland_en/p_study/prog_s/ucmapweb/ucmap_project/content/reports/final_report.pdf.
- Pongrácz, R., Bartholy, J., Zs. Dezső, 2010. Application of remotely sensed thermal information to urban climatology of Central European cities. *Phys. Chem. Earth* 35, 95–99. <https://doi.org/10.1016/j.pce.2010.03.004>.
- Pongracz, R., Bartholy, J., Bartha, E.B., 2013. Analysis of projected changes in the occurrence of heat waves in Hungary. *Adv. Geosci.* 35, 115–122. <https://doi.org/10.5194/adgeo-35-115-2013>.
- Pongrácz, R., Bartholy, J., Zs. Dezső, Cs. Dian, 2016. Analysis of the air temperature and relative humidity measurements in the Budapest Ferencváros District. *Hungarian Geographical Bull.* 65 (2), 93–103. <https://doi.org/10.15201/hungeobull.65.2.1>.
- Rasul, A., Balzter, H., Smith, C., Remedios, J., Adamu, B., Sobrino, J., Srivastav, M., Weng, Q., 2017. A review on remote sensing of urban heat and cool islands. *Land* 6 (2), 38. <https://doi.org/10.3390/land6020038>.
- Savić, S., Unger, J., Gál, T., Milošević, D., Popov, Z., 2013. Urban heat island research of Novi Sad (Serbia): A review. *Geographica Pannonica* 17 (1), 32–36 ISSN 0354-8724 (hard copy) | ISSN 1820-7138 (online).
- Schwarz, N., Lautenbach, S., Seppelt, S., 2011. Exploring indicators for quantifying surface urban heat islands of European cities with MODIS land surface temperature. *Remote Sens. Environ.* 115, 3175–3186. <https://doi.org/10.1016/j.rse.2011.07.003>.
- Stewart, I.D., 2007. Land scape representation and the urban-rural dichotomy in empirical urban heat island literatura, 1950–2006. *Acta Climatologica et Chorologica Universitatis Szegediensis, Tomus 40–41*, 111–121. <http://citeseerx.ist.psu.edu/viewdoc/download?doi=10.1.1.117.4203&rep=rep1&type=pdf>.
- Stewart, I.D., Oke, T.R., 2012. Local Climate Zones for urban temperature studies. *Bull. Am. Meteorol. Soc.* 93, 1879.1900. <https://doi.org/10.1175/BAMS-D-11-00019.1>.
- Strahler, A., Muchoney, D., Borak, J., Friedl, M., Gopal, S., Lambin, E., Moody, A., 1999. MODIS Land Cover Product Algorihm Theoretical Basis Document. Version 5. Center for Remote Sensing, Department of Geography, Boston University, Boston, MA, pp. 66. <https://pdfs.semanticscholar.org/8c83/49d66f9d663d7e7ccf9e0632edde719a1892.pdf>.
- Synop Riports, 2016. <http://www.ogimet.com/synops.shtml.en>.
- Tran, H., Uchihama, D., Ochi, S., Yasuoka, Y., 2006. Assessment with satellite data of the urban heat island effects in Asian mega cities. *Int. J. Appl. Earth Obs. Geoinf.* 8, 34.48. <https://doi.org/10.1016/j.jag.2005.05.003>.
- Unger, J., 2004. Intra-urban relationship between surface geometry and urban heat island: review and new approach. *Clim. Res.* 27, 253–264. <https://doi.org/10.3354/cr027253>.
- Unger, J., Lelovics, E., Gál, T., 2014. Local climate zone mapping using GIS methods in Szeged. *Hungarian Geographical Bull.* 63 (1), 29.41. <https://doi.org/10.15201/hungeobull.63.1.3>.
- United Nations, 2015. World Urbanization Prospects: The 2014 Revision, (ST/ESA/SER.A/366). UN Department of Economic and Social Affairs, Population Division, 517. <https://esa.un.org/unpd/wup/Publications/Files/WUP2014-Report.pdf>.
- Voogt, J.A., Oke, T.R., 2003. Thermal remote sensing of urban climate. *Remote Sensing Environ.* 86, 370–384. [https://doi.org/10.1016/S0034-4257\(03\)00079-8](https://doi.org/10.1016/S0034-4257(03)00079-8).
- Vukovich, F.M., 1983. An analysis of the ground temperature and reflectivity pattern about St. Louis, Missouri, using HCMM satellite data. *Journal of Appl. Meteorol.* 22, 560–571. [https://doi.org/10.1175/1520-0450\(1983\)022<0560:AAOTGT>2.0.CO;2](https://doi.org/10.1175/1520-0450(1983)022<0560:AAOTGT>2.0.CO;2).
- Wan, Z., Snyder, W., 1999. MODIS land-surface temperature algorithm theoretical basis document. Institute for Computational Earth Systems Science, University of California, Santa Barbara, pp. 77. <https://icess.eri.ucsb.edu/modis/atbd-mod-11.pdf>.
- WUDAPT, 2019. World Urban Database and Access Portal Tools. <http://www.wudapt.org/>.
- Yu, C., Hien, W.N., 2006. Thermal benefits of city parks. *Energy Build.* 38, 105–120. <https://doi.org/10.1016/j.enbuild.2005.04.003>.